HHS Public Access

Author manuscript

Nat Biotechnol. Author manuscript; available in PMC 2020 February 02.

Published in final edited form as:

Nat Biotechnol. 2019 August ; 37(8): 884–894. doi:10.1038/s41587-019-0205-0.

A divalent siRNA chemical scaffold for potent and sustained modulation of gene expression throughout the central nervous system

Julia F. Alterman[1,#], **Bruno M.D.C. Godinho**[1,#], **Matthew R. Hassler**[1,#], **Chantal M. Ferguson**[1,#], **Dimas Echeverria**[1], **Ellen Sapp**[3], **Reka A. Haraszti**[1], **Andrew H. Coles**[1], **Faith Conroy**[1,4], **Rachael Miller**[1,4], **Loic Roux**[1], **Paul Yan**[1], **Emily G. Knox**[1], **Anton A. Turanov**[1], **Robert M. King**[5,6], **Gwladys Gernoux**[7], **Christian Mueller**[7,8], **Heather L. Gray-Edwards**[5], **Richard P. Moser**[9], **Nina C. Bishop**[10], **Samer M. Jaber**[10,11], **Matthew J. Gounis**[5], **Miguel Sena-Esteves**[7,12], **Athma A. Pai**[1], **Marian DiFiglia**[3], **Neil Aronin**[1,4], **Anastasia Khvorova**[1,2]

[1]RNA Therapeutics Institute, University of Massachusetts Medical School

[2]Department of Molecular Medicine, University of Massachusetts Medical School

[3]Department of Neurology, Massachusetts General Institute for Neurodegenerative Disease

[4]Department of Medicine, University of Massachusetts Medical School

[5]Department of Radiology, New England Center for Stroke Research, University of Massachusetts Medical School

[6]Department of Biomedical Engineering, Worcester Polytechnic Institute

[7]Horae Gene Therapy Center, University of Massachusetts Medical School

[8]Department of Pediatrics, University of Massachusetts Medical School

[9]Department of Neurosurgery, University of Massachusetts Medical School

[10]Department of Animal Medicine, University of Massachusetts Medical School

[11]Department of Pathology, University of Massachusetts Medical School

[12]Department of Neurology, University of Massachusetts Medical School

Abstract

Corresponding Author: Anastasia Khvorova (Anastasia.khvorova@umassmed.edu; 774-455-3638 / 508-856-6696 (fax)). University of Massachusetts Medical School, 368 Plantation Street, Worcester, MA, 01605.

[#]These authors contributed equally to this work.

AUTHOR CONTRIBUTIONS

J.F.A., B.M.D.C.G., M.R.H., and A.K. conceived of the project. J.F.A., B.M.D.C.G., M.R.H., C.M.F., M.D, N.A. and A.K. contributed to experimental design. J.F.A., B.M.D.C.G., C.M.F, E.S., C.M.F., R.A.H., A.H.C., F.C., R.M., and L.R., P.Y., A.A.T., E.G.K., A.A.P., contributed experimentally. M.R.H. and D.E. synthesized the compounds. J.F.A., B.M.D.C.G., C.M.F., A.H.C., R.M.K., H.L.G.E., R.P.M., N.C.B., S.M.J., M.J.G., and M.S.E. carried out large animal studies. G.G. and C.M. provided naïve non-human primate samples. J.F.A., B.M.D.C.G., M.R.H., C.M.F. and A.K. wrote the manuscript.

This work was done in Worcester, Massachusetts, United States of America.

COMPETING FINANCIAL INTEREST STATEMENT

AK, JFA, MRH and BMDCG have filed a patent application for branched-oligonucleotides.

Sustained silencing of gene expression in deep regions of the brain using small interfering RNAs (siRNAs) has not been achieved. Here we describe an siRNA architecture, divalent-siRNA (Di-siRNA), that supports potent, sustained gene silencing in the central nervous system (CNS) of mice and non-human primates following a single injection into cerebrospinal fluid. Di-siRNAs are composed of two fully chemically modified, phosphorothioate-containing siRNAs connected by a linker. In mice, Di-siRNAs induced potent silencing of huntingtin, the causative gene in Huntington's disease, reducing mRNA and protein throughout the brain. Silencing persisted for at least six months, with the degree of gene silencing correlating to guide strand tissue accumulation levels. In Cynomolgus macaques, a bolus injection of Di-siRNA showed substantial distribution and robust silencing throughout the brain and spinal cord without detectable toxicity and with minimal off-target effects. This siRNA design may enable RNAi-based gene silencing in the CNS for the treatment of neurological disorders.

Introduction

Oligonucleotide therapeutics are an emerging class of drugs that enable potent and efficient modulation of gene expression *in vivo*[1]. An outstanding challenge is developing chemical architectures of oligonucleotides that permit robust, productive, and safe delivery to a particular target tissue. Small interfering RNA (siRNA) and antisense oligonucleotide (ASO) delivery and functionality have been established for the liver[2, 3], so recent efforts have shifted towards delivery to the central nervous system (CNS)[4,5].

siRNAs are large, negatively-charged, double-stranded molecules that require formulation[6] or chemical conjugation[7–10] for delivery to tissues (especially CNS). When fully chemically-stabilized siRNAs are conjugated to hydrophobic ligands like cholesterol[7], docosahexaenoic acid (DHA)[8], or DHA with a phosphocholine head group[10], they are successfully internalized by brain cells[11]. However, they are retained near the brain injection site, even with continuous monthly administration[4, 7]. Thus, other modification strategies are needed to expand siRNA distribution and efficacy in the CNS.

Broad distribution of ASOs, systemically and in the CNS, has been achieved primarily using phosphorothioate (PS) backbone modifications[12]. The most advanced CNS-active ASO scaffold utilizes a mixed backbone configuration with at least 70–80% PS content. This modification maintains efficacy and distribution with minimal risk of toxic phenotypes [13, 14] via mechanisms that are not fully understood[15]. PS modifications are also essential for clinically-advanced siRNA configurations[1, 16]. However, increasing the PS content of individual siRNA duplexes to 80% can limit RNA-induced silencing complex (RISC) efficacy [17, 18] and increase toxicity[19, 20].

An alternative approach may be multi-valency—i.e., cooperative interactions between multiple partially PS-modified siRNAs. Indeed, the most clinically-advanced siRNA conjugate is the multi-valent N-acetylgalactosamine (GalNAc)[21], which drives delivery to and silencing in the liver. A single subcutaneous injection of trivalent GalNAc-conjugated siRNA can achieve efficacy for >12 months[22, 2324].

Here we describe a divalent chemical scaffold of fully chemically modified, PS-containing siRNAs (Di-siRNAs) that provide widespread distribution and sustained gene silencing in rodent and non-human primate (NHP) brain after a single administration into cerebrospinal fluid (CSF). To characterize the novel scaffold, we used an siRNA sequence targeting huntingtin, the causative gene in Huntington's disease (HD) [4].

Results

Structure and synthesis of Divalent siRNAs

As full chemical modification of siRNAs is essential for conjugate-mediated delivery[16], we used fully chemically modified asymmetric siRNAs that have a 20-base guide strand and 15-base passenger strand. All terminal backbone positions and the protruding 3' end of the guide strand are fully phosphorothioated, resulting in PS modifications to 13 out of 35 phosphate linkages (~40% PS content) (Fig. 1a). These unconjugated siRNAs exhibit minimal brain retention and distribution (Fig. 1b).

Di-siRNA was synthesized using a functionalized solid support (Supplementary Fig. 1), which allowed for parallel growth of two oligonucleotides. As a result, two sense strands are covalently connected at their 3'end through a tetra-ethylene glycol (TEG) linker. Use of the polymeric spacer was necessary to limit steric hindrance during synthesis and functional knockdown. Annealing of the passenger strand to two identical 20-base guide strands formed a ~27 kD compound (Fig. 1c). Mono- and Di-siRNAs show comparable *in vitro* IC50 values (Supplementary Fig. 2), suggesting that linking the two molecules does not compromise RISC loading. The sequences and chemical configuration of all compounds used in this study are shown in Supplementary Table 1.

Di-siRNA shows widespread retention after an intra-parenchymal injection

Intra-parenchymal injection of Cy3-labeled Di-siRNA significantly enhanced distribution and retention in the mouse brain compared to Cy3-labeled monovalent siRNA (Fig. 1d), supporting the idea that a cooperative interaction between two partially PS-modified siRNAs is sufficient for widespread brain retention. In all experiments, the dose of injected compounds (Mono- vs Di-siRNA) was defined by guide strand concentration (i.e., Di-siRNA injection includes half the number of molecules compared to the Mono-siRNA injection).

Di-siRNA targeting huntingtin (*Htt*) mRNA was synthesized using a previously identified siRNA sequence[7]. Intra-striatal injection of Di-siRNA^{HTT} in wild type mice resulted in potent down-regulation of *Htt* mRNA (between 50–75%) in the striatum and cortex two weeks after injection (Supplementary Fig. 3a). Both Cy3-labeled and non-labeled Di-siRNA^{HTT} show similar levels of silencing in cortex and striatum (~80% silencing, $p < 0.0001$, Supplementary Fig. 3b), whereas the non-targeting control (NTC) oligonucleotide did not impact target gene expression (Supplementary Fig. 3a–b).

We also synthesized Di-siRNA^{HTT} variants containing fewer and no PS backbone modifications (Supplementary Fig. 4a). Reducing the number of PS modifications reduced silencing efficacy, and completely removing PS modifications fully abolished activity

(Supplementary Fig. 4b), after intra-striatal injection in mice. Thus, the observed efficacy of Di-siRNA^{HTT} is phosphorothioate mediated.

Di-siRNA distributes broadly with productive silencing after a bolus CSF injection

To evaluate CSF-driven brain distribution of Cy3-Di-siRNA, we injected 475 μg intracerebroventricularly (ICV) into the lateral ventricles of mice. Forty-eight hours after the injection, the mouse brain was uniformly pink to the naked eye (Fig. 1e), indicating broad distribution. Microscopy confirmed our initial observation (Fig. 1f). Di-siRNAs distributed to all regions of the brain—from the prefrontal cortex to the cerebellum. High magnification images show accumulation in the vast majority of neurons (Fig. 1g,h). Intracellular distribution followed a perinuclear localization pattern that is characteristic of oligonucleotides[11].

Broad distribution of Di-siRNA^{HTT} supported productive silencing two weeks post injection in all brain regions, including prefrontal, medial and posterior cortices, striatum, hippocampus, thalamus, hypothalamus, cerebellum, brain stem and cervical, thoracic, and lumbar sections of the spinal cord (Supplementary Fig. 5). To quantitatively evaluate guide strand accumulation, we used a PNA hybridization assay, which provides quantitative accumulation data and does not depend on the presence of a fluorescent label[25]. Analysis (Supplementary Fig. 5a) confirmed the visual and microscopy-based observations of broad Di-siRNA distribution, and correlated with *Htt* mRNA (Supplementary Fig. 5b) and HTT protein (Supplementary Fig. 5c,d) silencing.

Next, we compared the efficacy of two different Di-siRNA^{HTT} doses—60 and 475 μg—one month after injection in wild type mice (Supplementary Fig. 6a). The higher dose resulted in approximately a two-fold maximum increase in guide strand tissue retention and a wider distribution compared to the lower dose (0.1 to 4 μg/g at 60 μg; 2–8 μg/g at 475 μg dose, Supplementary Fig. 6b). The higher dose silenced HTT protein below level of detection ($p < 0.0001$) throughout the brain (Fig. 1i; Supplementary Fig. 7). The lower dose was efficacious in the hippocampus, thalamus, and striatum, showing 80–99% silencing ($p < 0.0001$, $p < 0.001$, $p < 0.0001$, respectively). Efficacy was reduced in the cortical areas located away from the site of injection, consistent with the relatively lower guide strand accumulation in these regions. NTC and PBS groups showed no difference in HTT expression level. NTC was used as a control for all subsequent experiments (Fig. 1i).

Di-siRNA can be reprogrammed to silence multiple genes in the CNS

The chemical architecture of an siRNA determines pharmacokinetics and tissue delivery, but the base sequence of the oligonucleotide determines its target. To evaluate the programmability of the Di-siRNA scaffold, we measured its efficacy when targeted to other mRNAs in the CNS.

Upon intra-striatal injection of Di-siRNA targeting Cyclophilin B (*Ppib*), we observed potent *Ppib* silencing (65–85%, $p < 0.0001$; Supplementary Figure 8). The NTC control had no activity, demonstrating that silencing was specific to the PPIB-targeting sequence. Recently, we identified functional siRNA sequences targeting Apolipoprotein E (ApoE), implicated in several neurodegenerative diseases, including Alzheimer's disease and

Amyotrophic Lateral Sclerosis[26–28] (Ferguson *et al.*, manuscript in preparation). We synthesized Di-siRNA^{ApoE} (see Supplementary Table 1 for sequence information) and injected mice ICV with PBS and NTC as controls. Figure 1j (Supplementary Fig. 10 for raw westerns) shows that a single CSF injection of Di-siRNA^{ApoE} resulted in potent silencing (> 95%) of APOE protein after one month. NTC had no impact on APOE expression, indicating that observed silencing is sequence specific and not caused by the Di-siRNA chemical scaffold. The observed protein silencing correlated well with mRNA silencing (Supplementary Fig. 10). Thus, the Di-siRNA chemical scaffold can be reprogrammed to modulate gene expression *in vivo* for multiple targets implicated in the pathogenesis of neurological conditions.

The efficacy of high-dose Di-siRNA exceeds six months

To evaluate the duration of Di-siRNA efficacy, we delivered a high dose (475 μg) of Di-siRNA^{HTT} or Di-siRNA^{NTC} to wild type mice via a single ICV injection. We measured guide strand accumulation levels, *Htt* mRNA, and HTT protein in key brain regions (cortex, striatum, thalamus, hippocampus) at one, four, and six months post injection (Fig. 2a). Guide strand accumulation in different brain regions ranged between 2–7 μg/g at one month, 0.8–2.5 μg/g at four months, and 0.2– 1.8 μg/g at six months, suggesting relatively slow clearance (Fig. 2b).

The extent of HTT protein silencing was always greater than *Htt* mRNA (> 99% vs ~70%) (Fig. 2c,d) because a fraction of *Htt* mRNA localizes to the nucleus, making it more resistant to RNAi-based silencing[29]. More than 80% silencing of HTT protein was maintained at four months in all brain regions analyzed (Fig. 2d, Supplementary Figures 7, 11 for raw westerns). At six months, the degree of silencing differed between brain regions: > 90% in hippocampus, ~50% in thalamus and striatum, and high variability in the cortex.

Di-siRNA retention correlates with mRNA and protein silencing

Using data from all time points in the duration of effect study, we observed strong correlations between the level of residual guide strand accumulation and the degree of *Htt* mRNA (Fig. 2e) and HTT protein (Fig. 2f) silencing. We estimate the protein silencing IC50 value to be ~0.5 μg/g and the IC90 value to be ~2 μg/g of guide strand accumulation in tissue.

Figure 2g shows guide strand clearance over time for individual brain regions. Initial (one month) hippocampal accumulation of ~7 μg/g resulted in ~2 μg/g present at 6 months. Both levels of guide strand accumulation are sufficient to silence HTT protein below the level of detection. In the cortical regions, initial accumulation at one month was 3–4 μg/g and fell below the 0.5 μg/g threshold by six months, resulting in loss of silencing in some animals. This suggests that siRNA tissue accumulation at early time points can be used to estimate duration of effect.

Di-siRNA are safe and well-tolerated in mice

Next, we evaluated overall safety and tolerability of Di-siRNA at 475 μg over 6 months. To assess neuronal viability, we measured DARPP32 protein expression, an established marker

for medium spiny neurons in the striatum[7]. Loss of DARPP32 indicates neuronal death. Injection of Di-siRNA had no impact on DARPP32 expression (Supplementary Fig. 7, 11). To evaluate the impact of Di-siRNA injection on microglia activation and gliosis, we measured two well-established markers of immune stimulation, IBA-1 and GFAP. IBA-1 is located within a major histocompatibility complex and increases as a result of microglial activation[7]. GFAP is an intermediate filament protein and increases as a result of astrocyte proliferation[30]. We observed only minor changes in *Iba-1* expression (<1.5 fold from control) at both doses and at all three time points. At the higher dose, we observed transient *Gfap* activation at one month, but this disappeared by four months (Supplementary Fig. 12, 13). Finally, a comprehensive blood chemistry panel showed no detectable changes at any time point, suggesting a systemic tolerability of Di-siRNA administration to the CNS (Supplementary Fig. 14). Overall, Di-siRNA injection in CSF was well tolerated in mice at the doses and time points tested.

Di-siRNA silences wild type and mutant HTT protein with similar efficiency

Di-siRNA^{HTT} is perfectly complementary to both human *HTT* and mouse *Htt* genes[7]. To evaluate the ability of Di-siRNA^{HTT} to silence mutant *HTT*, we measured efficacy in the BACΔN17 mouse model of HD. This HD model contains wild type mouse *Htt* and mutant human *HTT* (97 CAG repeats) with 17 N-terminal amino acids removed[31]. At seven weeks old, animals were injected with 475 μg Di-siRNA targeting *HTT* or NTC, or with PBS. HTT protein expression was evaluated at five months of age (~three months post injection). We used a combination of two antibodies (Ab1 and 1C2) to evaluate specific knockdown of wild type mouse and mutant human HTT protein. The Ab1 antibody only detects wild type HTT protein, as its epitope is located in exon 1[32]. The 1C2 antibody detects polyQ expansions[33]; and thus, is specific to the mutant protein. A single injection of Di-siRNA^{HTT} showed potent down-regulation of both mutant and wild type HTT protein (Supplementary Fig. 15), with a silencing efficiency similar to that in wild type mice at four months post injection (Fig. 2d). This finding suggests that Di-siRNA can be used to silence both mutant and wild type *HTT* expression.

Di-siRNA distributes and silences in NHP brain

Rodent systemic distribution is generally predictive of large mammal distribution. However, this is not necessarily the case for the CNS. Complexity of brain structure, CSF volume, rate of clearance, and the overall distance of brain regions from the CSF may contribute to oligonucleotide distribution and retention. We evaluated the distribution, efficacy, and safety of a single CSF injection of Di-siRNA in the Cynomolgus macaque, whose siRNA-targeting region in the *HTT* sequence is equivalent to that in mouse and human.

We delivered Di-siRNA^{HTT} via ICV injection, using Magnetic resonance Imaging (MRI) and Computerized Tomography (CT) to confirm needle placement in the lateral ventricle. A 25 mg dose in 750 μl of PBS was infused over 10 minutes (see Methods). Animals woke up within 15 minutes after anesthesia was discontinued, with no observable adverse events. Figure 3a shows a schematic of the study timeline. Forty-eight hours after unilateral injection, we observed uniform distribution throughout the non-human primate (NHP) brain, similar to mice. The injected oligonucleotide was fluorescently labeled, allowing for visual

and microscopy-based distribution evaluation. The brain appeared visibly pink with no obvious difference in the degree of oligonucleotide distribution in injected vs non-injected sides (Fig. 3b). Upon sectioning of the brain, we observed uniform cortical distribution with evident delivery to deep brain structures, including the striatum (caudate and putamen) and hippocampus (Fig. 3c). Fluorescent microscopy confirmed the visual distribution, with significant delivery to the cortex, caudate, and hippocampus.

To evaluate any potential preference for specific cell-types, we performed immunofluorescence on sections of Di-siRNA-treated NHP brains using neuron-specific (NeuN)[34] and glial cell-specific (GFAP)[35] antibodies. We observed efficient distribution of Di-siRNA to both neurons and glial cells in the hippocampus and cortex, and observed co-localization of Di-siRNA (red) with both neurons (green) and glial cells (purple) (Fig. 3d). This finding suggests that Di-siRNA could be used to treat neurological conditions affecting multiple cell types.

At one-month post injection (Fig. 3e), we observed 1–9 μg/g guide strand accumulation, with the highest accumulation detected in the cortex (9 μg/g), hippocampus (6 μg/g), and thalamus (6 μg/g), and the lowest accumulation in the caudate (2 μg/g) and putamen (1 μg/g). Supplementary Figure 16 shows cortical accumulation across seven slices spanning the entire brain (both ipsilateral and contralateral biopsies), confirming microscopy observations. In all NHP brain regions, guide strand accumulation level was well above the established IC50 value of ~0.5 μg/g (Fig. 2f).

To evaluate Di-siRNA^{HTT} efficacy, we assessed *HTT* mRNA and protein expression in the NHP brain one-month after injection. We observed potent silencing of mRNA expression in all brain regions, independent of the normalization control used (*PPIB* or *HPRT)*, Supplementary Fig. 17). There was no major difference in silencing between the ipsilateral and contralateral sides of the brain, which is consistent with uniform distribution. For protein silencing (Fig. 3f, Supplementary Fig. 18 for raw westerns), we observed >90% silencing in cortex ($p < 0.001$), >80% silencing in hippocampus ($p < 0.01$), ~50–85% silencing in the caudate ($p < 0.001$), and ~40–70% silencing in putamen ($p < 0.05$). These data indicate that a single injection of Di-siRNA enables silencing of target gene expression throughout the NHP brain.

Di-siRNA distributes and silences in NHP spinal cord

The cortex and striatum are the two brain regions primarily affected in HD. However, treatment of other neurodegenerative disorders (e.g. ALS) may require gene modulation in the spinal cord. We evaluated Di-siRNA distribution and efficacy throughout the spinal cord one-month post injection (Fig. 4). We observed robust distribution to all spinal cord regions, with guide strand accumulation ranging from 4–7 μg/g (Fig. 4d). Slightly higher accumulation was seen in the lumbar compared to the cervical region. In all sections tested, we observed efficient delivery to all cell types, including neurons. Figure 4c shows immunofluorescent images of the ventral horn of the lumbar spinal cord segment, indicating robust delivery to lower motor neurons, easily identified morphologically by their large soma. Again, the level of guide strand accumulation was sufficient for potent *HTT* mRNA

silencing in all regions tested ($p < 0.01$), with the exception of a single outlier in cervical white matter (Fig. 4e).

Absence of detectable adverse events.

We next looked at overall safety and tolerability of a single injection of 25 mg Di-siRNA in NHP. MRI is commonly used to look at brain inflammation and edema. MRIs were collected pre-operatively and one month following injection. There was no detectable difference between these scans, indicating that Di-siRNA injection did not cause a major inflammatory response (Fig. 5a). Consistent with this finding, we observed no significant up-regulation of *IBA-1* and *GFAP* at one month post injection (Fig. 5b,c). To determine whether there was any effect on neuronal viability, we examined two additional markers by western blot, NeuN[36] and BF-1[37]. We observed no differences between naïve and treated animals (Supplementary Fig. 19). In addition, we found no measurable changes in blood chemistry or cell counts (Supplementary Fig. 20), which is particularly important because thrombocytopenia (low platelet count) has been reported as a PS-mediated rare adverse event[13, 14].

Finally, we sent treated and naïve NHP brain sections for independent neuropathological analysis (Supplementary Note 2). The summary of the report is included in Supplementary material. No histopathological changes, with exception of changes resulting directly from the needle track, were identified.

Di-siRNA modulates *HTT* expression with minimal off-target events

To determine if *HTT* silencing or Di-siRNA treatment had any major effect on the transcriptome, we performed genome-wide RNA sequencing (RNA-seq), comparing Di-siRNA^{HTT}-treated to naïve NHP brains. We analyzed three cortical replicates from each of 8 animals (4 naïve, 4 treated). We chose to analyze the cortex, because we observed the highest accumulation of Di-siRNA in this region. Therefore, the chances of seeing off-target effects would be maximized.

We observed 52 genes with significant differential expression between treated and naïve animals, using a 1% False Discovery Rate (FDR) significance threshold (Figure 6a, Supplementary Table 2). As expected, *HTT* was a single outlier with the most significantly impacted mRNA levels (75% silencing, $P < 10^{-40}$). Most other gene expression changes were minimal.

siRNA off-target effects are a major concern in development of siRNA-based therapeutics[38]. siRNA off-target effects are predominantly due to seed (position 2–7 of the guide strand) complementarity in the 3' UTR of other targets[39]. To evaluate if the observed non-*HTT* gene expression changes were due to off target effects of the siRNA, we looked at enrichment for seed complementarity in significantly downregulated and upregulated targets. Downregulated transcripts were slightly enriched for perfect complementarity to the guide strand seed region ($P = 0.04$) while no enrichment was observed in up-regulated genes ($P = 0.59$). No enrichment was observed for seed reverse complement. The off target effects observed in this study are minor in comparison to a previous study evaluating RNA-seq data in siRNA-treated rat liver[38].

To look more broadly at potential seed enrichment, we searched all differentially expressed 3' UTRs for any combination of six nucleotides (seed length) that were overrepresented. For genes differentially expressed at a 1% FDR, there were no significantly over-represented 6-mers and the HTT siRNA seed complement, AGAUUA, was present in the middle of the distribution (Fig. 6b). Relaxing the differential expression threshold to 10% FDR, there were several overrepresented 6-mers, but none of them matched AGAUUA (Supplementary Fig. 21).

There were 7 differentially expressed genes whose 3' UTRs contain the AGAUUA seed complement. The gene expression values (transcripts per million) for individual animals are shown in Figure 6c. For five out of seven transcripts, the changes were minor and are likely not biologically significantly. Thus, there were only two potential genes, *APOLD1* (~ 40% down) and *ANLN* (~ 20% down), that may be down-regulated due to miRNA-like off-target silencing.

HTT is involved in several cellular processes[40], raising the potential for transcriptional changes downstream of HTT silencing (on-target vs off-target effects). To determine if changes were due to on-target effects of HTT silencing, we performed gene ontology analyses on the differentially expressed genes. With a 1% FDR, only the "immune system processes" category was significantly enriched among differentially expressed genes, with 12 out of 576 expressed genes in this category showing differential expression.

With a 5% FDR, three other pathways were slightly significantly enriched (Fig. 6d): G-protein-coupled purinergic receptors signaling, adenosine receptor signaling and purinergic receptor signaling. It is currently unknown whether the observed minor transcriptional changes are of biological significance and, if so, whether they were caused by the trauma of ICV injection, HTT silencing, or off-target silencing. In general, RNA-seq analyses of Di-siRNA^{HTT} treated NHP brains reveal no major transcriptional changes (aside from *HTT* silencing) and minimal, if any, off-targeting activity. Thus, Di-siRNA enables highly-specific silencing of gene expression in the CNS.

Discussion

Many technologies are being explored for gene modulation in the CNS, including adeno-associated virus (AAV) and ASOs[4, 41, 42]. AAV delivered by intra-parenchymal injections efficiently silenced HTT in minipig, sheep, and NHP [41, 43, 44]. However, multiple injections of AAV are required due to the limited distribution achieved with a single injection. Major advances in AAV delivery are needed for uniform silencing throughout the brain. ASOs have enabled ~50% decrease of soluble mutant HTT in the CSF of patients following monthly intrathecal injections[45]. However, ASO delivery to deep brain structures is limited[4], with no significant HTT silencing observed in NHP caudate after multiple injections[42].

We have shown that divalent, PS-containing, fully chemically modified siRNAs achieve widespread distribution and silencing after a single bolus injection in rodent and NHP brains. Bulk flow of CSF is thought to be the primary mechanism driving broad oligonucleotide distribution and clearance in the brain. Thus, the difference in size between

ASOs (7 KD) and Di-siRNAs (27 KD) may contribute to the difference in distribution to deep brain structures. Linking of two ASOs via their 5' ends resulted in better systemic efficacy compared to monomeric ASO variants[46].

Di-siRNAs are comprised of two PS-containing siRNAs, with 26 PS modifications per molecule. Elimination of PS content completely abolished efficacy (Supplementary Fig. 4), suggesting that enhanced brain retention and distribution depends on PS modifications. The underlying mechanism is not fully understood, but multiple cell surface receptors have been recently identified that may be involved in phosphorothioate-mediated oligonucleotide uptake[15]. Our findings are consistent with recent efforts to fine-tune ASO potency and toxicity profiles via optimization of PS content (Moazami et al., in review). The level of PS modification in each strand of Di-siRNAs (~40% phosphorothioated) is not sufficient to promote significant retention of monomers. Yet, by increasing the size and linking two siRNAs, the cooperativity of weak PS-driven cellular interactions produces robust cellular uptake and retention. Since increasing the percentage of PS modifications in the siRNA, either uniformly (i.e. every other nucleotide linkage) or strategically, may interfere with RISC [17, 18] and reduce tolerability, a multi-valency approach may be preferable for fine-tuning siRNA uptake and toxicity.

We show that, in mice, duration of effect can be predicted based on compound tissue accumulation at earlier time points (one month). In NHPs, we observed potent silencing in all brain regions at one month after injection. Given the level of accumulation in cortex and hippocampus, silencing is expected to last 6–9 months in these regions, and as long as 2–4 months in the caudate and putamen. Therefore, repetitive injections would be necessary to maintain *HTT* silencing throughout the brain.

Animals with a single treatment of Di-siRNA targeting *HTT* showed significant silencing of *HTT* with minimal transcriptome-wide changes. miRNA-like off-target effects were observed for only two genes. Although seed complementary sequences were slightly overrepresented in the 3' UTRs of downregulated transcripts, the overall effect and degree of enrichment was minimal compared to previously observed off-target effects with siRNA in rat livers[38] and in cells[47]. Off-target effects were explored in cortical samples, where guide strands accumulated to more than 9 μg/g and resulted in > 90% HTT protein silencing. Substantially lower accumulation is sufficient for target silencing; therefore, the minimal off-target effects in this region are likely representative of transcriptome changes at high guide strand concentration. It is unclear whether the minimal level of off-target effects is specific to CNS regions, NHPs, or these particular compounds because no other genome-wide off-targeting data in NHPs are available for comparison. However, our findings are consistent with published data in adult mice demonstrating that eliminating HTT causes minimal off-target phenotypes[48]. Although, lack of major transcriptional changes is consistent with the notion that there is no major perturbation of miRNA machinery, further investigations are required to detect changes in small RNA function.

It is currently unclear whether non-selective or single nucleotide polymorphism (SNP)-selective *HTT* silencing is a better therapeutic strategy for HD. However, a non-selective strategy would allow for treatment of all HD patients with a single entity[49]. Di-siRNA is

delivered to most cortical neurons, resulting in non-selective, potent silencing of wild type and mutant HTT in the CNS, independent of brain size. Further evaluation in established disease models is necessary to assess the safety and efficacy of Di-siRNA-mediated silencing of HTT and other targets.

Online Methods

Oligonucleotide synthesis, deprotection and purification

Oligonucleotides were synthesized using modified (2′-F, 2′-OMe) phosphoramidite with standard protecting groups. Solid-phase synthesis conditions using a MerMade 12 (BioAutomation, Irving, Texas) or AKTA Oligopilot 100 (GE Healthcare Life Sciences, Pittsburgh, PA) using modified protocols. Unconjugated antisense oligonucleotide strands were grown on controlled pore glass functionalized with a long-chain alkyl amine and Unylinker® terminus (Chemgenes, #N-4000–10) Sense strands, as divalent oligonucleotides were synthesized on modified solid support **(5)**, made in house to produce di-valent sense strands. Phosphoramidites (ChemGenes, Wilmington, MA) were prepared at 0.15M (MerMade 12) and 0.2M (AKTA) in ACN with added 15% DMF in the 2`-OMe U amidite. 5-(Benzylthio)-1H-tetrazole was used as the activator at 0.25M. Detritylations were performed using 3% trichloroacetic acid (TCA) in dichloromethane on the MerMade 12 and 3 %DCA in toluene on the AKTA Oligopilot (AIC Wilmington, MA). Capping was done with non-THF containing reagents CAP A: 20% NMI in CAN and CAP B: 20% Ac2 O, 30% 2,6-lutidine in CAN (AIC Wilmington, MA). Sulfurization was performed with 0.1 M solution of DDTT in Pyridine (ChemGenes, Wilmington, MA) for 3 minutes. Phosphoramidite coupling times were 8min for all amidites used.

Vinyl phosphonate deprotection

The vinylphosphonate (VP) containing oligo, while still on solid support, post synthesis was treated with a mixture of trimethylsilyl bromide/DMF/pyridine (1:9:0.5) for 1 hour at room temperature with gentle agitation. The CPG is then rinsed with 10ml DMF followed by 10ml of water, 10ml ACN and allowed to dry. Before being deprotected normally as described below.

Deprotection and purification of oligonucleotides

Both sense and antisense strands were cleaved and deprotected using 40% aq. methylamine at 45 °C for 60 minutes. The oligonucleotide solutions were then cooled in a freezer for a few minutes and filtered to remove the CPG from the cleaved oligo. The filtrate was then cooled with dry ice then dried under vacuum in a Speedvac. The resulting pellets were re-suspended in 5% ACN in water. The purification of antisense strands was performed on an Agilent 1100 series system, equipped with an Agilent PL-SAX, polymer ion exchange column (50×150mm), or sourceQ anion exchange resin (GE healthcare Chicago IL) (50×200mm custom packed column) using the following conditions, Eluent A: 20% ACN 20mM NaAc pH 8, Eluent B: 1M sodium perchlorate in 20% ACN, gradient: 0% B 2min, 35% B 12min, clean and re-equilibration to initial conditions at 50ml/min. Purification of sense strands was performed on the same equipment but equipped with a PRP-C18, a polymer reverse phase column (4.6×150mm), using the following conditions, Eluent A: 50

mM sodium acetate in 5% ACN, and eluent B: ACN, gradient: 0% B 2min, 0–40% B 1min, 40–70% B 8min, clean and re-equilibration 6min. Temperature 70°C, and flow rate, 50 ml/min, were the same in both cases. Peaks were monitored at 280nm. The pure oligonucleotides fractions were collected, individually characterized by LCMS, combined, frozen and dried in a speedvac overnight. Oligonucleotides were re-suspended in 5% ACN, and desalted through fine Sephadex® G-25 columns (50mmx300mm), and lyophilized. All reagents mentioned above were purchased form sigma Aldrich and used as is, unless otherwise stated.

LC-MS analysis of oligonucleotides

The identity of oligonucleotides were established by LC-MS analysis on an Agilent 6530 accurate mass Q-TOF LC/MS machine using the following conditions, Buffer A: 100mM HFIP/9mM TEA in LC/MS grade water, Buffer B: 100mM HFIP/9mM TEA in LC/MS grade methanol, column: Agilent AdvanceBio oligonucleotides C18, gradient antisense: 0% B 1min, 0–30% B 8min, clean and re-equilibration 4min, gradient sense: 0% B 1min, 0–50% B 0.5min, 50–100% B 8min, clean and re-equilibration 4min, temperature: 45°C, flow rate: 0.5mL/min, UV (260nm). MS parameters, Source: ESI, ion polarity: negative mode, range: 100–3200 m/z, scan rate: 2 spectra/s, VCap: 4000, fragmentor: 180V. All reagents mentioned above were purchased form sigma Aldrich and used as is, unless otherwise stated.

Cell culture and in vitro screening

As described previously in Hassler et.al. NAR 2018. Briefly, HeLa cells were treated with RNAiMax (13778–150) formulated Mono-siRNAs and Di-siRNAs for 72 hours in 50/50 DMEM (Cellgro, 10–013-CV)/OptiMEM (Gibco, 31985–070) with 3% FBS and no PS. Cells were then lysed in diluted lysis mixture,1:2 lysis mixture (Invitrogen, 13228):water with proteinase K (invitrogen, 25530–049). mRNA was detected according to the Quantigene 2.0 protocol using the following probesets: human HTT (SA-50339), human HPRT (SA-10030).

Animal Studies

All experimental studies involving animals were approved by the University of Massachusetts Medical School Institutional Animal Care and Use Committee (IACUC Protocol #A-2411 and #A-2515) and performed according to the guidelines and regulations therein described.

Stereotactic injections in rodents

FVB/NJ females (8–9 weeks old) or BACHD-ΔN17 females (6 weeks old) were anesthetized using 1.2% Avertin. Single intrastriatal administrations (2 μL, per injected side) were performed as previously described[8, 10] at the following coordinates from bregma: +1.0 mm anterior-posterior (AP), +/−2.0 mm medio-lateral (ML) and −3.0 mm dorso-ventral (DV). Single bilateral intracerebroventricular injections (5 μL, per injected side) were performed at 500 nl/min after needle placement at the following coordinates from bregma:

−0.2 mm AP, ±0.8 mm ML and −2.5 mm DV. Doses of Mono-siRNA and Di-siRNA ranged between 4 nmol (50 μg) and 40 nmol (475 μg) according to the goal of the experiment.

For biodistribution studies, animals (n = 2–3/group) were euthanized at 48 hours after injection and perfused with PBS. Brains were harvested and post-fixed overnight with 10% formalin and processed for paraffin embedding. For efficacy studies, animals (n = 6–8/group) were euthanized at different time points, including 1, 2 weeks and 1, 3, 4, 6 months after single intracranial injections. At harvesting, tissues were kept in RNA later overnight (mRNA analysis) and then stored in −80ºC, or snap frozen (western blot assessments) and stored.

Stereotactic injection in non-human primates

Cynomolgus macaques (2.5–4.5 Kg) were sedated using Ketamine (15 mg/kg), Xylazine (0.5 mg/kg) and Glycopyrolate (0.01 mg/kg), and a tracheal tube placed. Anesthesia was maintained by isoflurane 1 – 3% carried by oxygen (1 L/minute). Animals received intravenous lactate ringer solution (LRS) at a rate of 5–10 ml/kg/hr and were placed on a heating blanket. Meloxicam (0.15 mg/kg) and buprenorphine (0.01 mg/kg) were given for analgesia. Respiratory rate, end tidal CO_2, body temperature, spO_2 and heart rate were monitored and recorded.

Standard surgical aseptic technique was used throughout the procedure. Macaques were positioned on a stereotaxic frame for non-human primates (KOPF Model 1530M) and skin cleaned with alternating applications of betadine and alcohol. The skull was exposed by a transverse incision and the periosteum removed from the surgical area. Based on the positioning of Bregma a burr hole (3–5 mm) was drilled using a Stryker high-speed drill (Core Powered Instrument Driver and Precision Neuro drill bit (Cat. #5820–107-530)). Real-time Cone Beam Computerized Tomography (CBCT) images were registered on pre-operative Magnetic Resonance Imaging (MRI) data sets (see details on MRI acquisition below) for determination of correct positioning of the manipulator for cannula placement. Cannula was lowered to the left lateral ventricle, 50 μL of iodohexal contrast agent was administered followed by high-resolution CBCT to confirm correct positioning of the device. FDA-approved SmartFlow™ neuroventricular cannulas (16 ga, 0.008’’ ID x 4 ft, MRI Interventions, Inc) were used for all intracerebroventricular (ICV) injections. Cannulas were attached to a syringe fitted in a programmable PhD Ultrapump (Harvard Apparatus).

Di-siRNAs (25 mg/750 μL) were injected at a rate of 50 μL/min for 15 minutes, and anesthesia switched to Propofol (1 mL/hour). Cannulas were withdrawn 5–10 minutes after the end of the injections. The skull was irrigated with ~50 mL of 0.9% saline and scalp sutured with absorbable sutures (3–0 or 4–0 Vicryl Rapide) in an interrupted pattern. Animals were kept under anesthesia for ~2 hours following the end of the ICV injection and were given prophylactic antibiotics (Cephazolin, IV). Macaques were returned to their home cage to recover and monitored for signs of pain and distress.

Complete Blood Counts (CBC) and a comprehensive blood chemistry panel was carried out on pre-operative blood and after 2 days (distribution study), or 15-days and 30 days post-injection (efficacy studies). For siRNA guide strand quantification, blood samples were

collected pre-operatively and at the following time points after Di-siRNA injection: 5, 15, 30 minutes, 1 and 2 hours.

At necropsy animals where heparinized and euthanized with an intravenous injection of pentobarbital (150 mg/kg). CSF samples were immediately collected from the cisterna magna after euthanasia. Animals were then perfused with 4 L of sterile cold PBS, and tissues collected for mRNA, protein and histology.

Brain Magnetic Resonance Imaging

Pre-operative and 30-day MRI scans were acquired using a Philips Achieva 3Tesla Whole Body Scanner. Animals were anesthetized as previously described and placed on a MRI-compatible stereotaxic frame in ventral recumbency (head first into the magnet). Axial T1 unenhanced spin-echo, axial T2 fast spin-echo, diffusion weighted imaging, magnetic resonance angiography and magnetization prepared rapid gradient echo sequences. In-plane resolution was 0.4 to 1mm, slice thickness 1–4mm, and 256×256 acquisition matrix. Total MR imaging time was approximately 60–90 minutes per subject. Following imaging, the animal was recovered from anesthesia and monitored in cage.

mRNA quantification

Mouse brain tissue was harvested and placed in ice cold PBS (Fisher, BP2438). Brains were sliced into 300 μM sections on a vibratome. Two mm punches were taken from each section. Punches from the left side were put into RNAlater (Sigma, R0901) for mRNA quantification.

NHP brains were perfused with ice-cold PBS (Fisher, BP2438) prior to sectioning. Brains were sectioned in a brain matrix into 4 mm sections. 2 mm punches were taken from various brain regions and placed in RNAlater (Sigma, R0901) for mRNA quantification.

As described previously[16], tissues were lysed in Quantigene 2.0 homogenizing buffer (Invitrogen, QG0517) with proteinase K (invitrogen, 25530–049). mRNA was detected according to the Quantigene 2.0 protocol using the following probe sets: mouse HTT (SB-14150), mouse GFAP (SB-14051), mouse IBA1 (SB-3027744), mouse HPRT (SB-15463), mouse PPIB (SB-10002), mouse *ApoE* (SB-13611), NHP HTT (SF-10209), NHP GFAP (SF-4228397), NHP IBA-1 (SF-4214274), and NHP HPRT (SF-10356).

Protein quantification

Mouse tissue collection was performed as described above in the mouse mRNA tissue collection. Punches from the right side of brain were flash frozen for western blot preparation.

NHP tissue collection was performed as follows: NHP brains were perfused with PBS prior to sectioning. Brains were sectioned in a brain matrix into 4 mm sections. 2 mm punches were taken from various brain regions flash frozen for western protein quantification.

Tissue processing was performed as described previously[7].

For analysis of ApoE protein expression in mouse brain samples, WES by ProteinSimple was used. Tissue punches were collected as above and flash-frozen and placed at −80 C. After addition of RIPA buffer with protease inhibitors, samples were homogenized and stored at −80C. Protein amount was determined using Bradford Assay. Samples were diluted in 0.1x sample buffer (ProteinSimple) to ~0.2–0.4 ug/ul. Anti-ApoE antibody (Abcam, 183597) was diluted 1:200 in antibody diluent (ProteinSimple) and loading control, anti-Vinculin (Invitrogen, 700062), was diluted 1:600 in antibody diluent. Assay was performed as described by ProteinSimple protocol using the 16–230 kDa plate (SM-W004).

Guide strand quantification

Conducted as described previously[16]. Briefly, guide strand was quantified by hybridization to a complementary PNA strand labeled with a Cy3 fluorescent dye. Accumulation was then measured by HPLC fluorescence detection and peak quantification.

Fluorescent imaging

Conducted as described previously[16]. Briefly, tissues for imaging were fixed overnight in (mouse) or for 7 days (NHP) in 10% neutral buffered formalin (Sigma, HT501320), and then transferred to PBS. All tissues were paraffin imbedded and sliced into 4 μM sections. Sections were stained with DAPI and imaged on a Leica inverted microscope. Staining for colocalization of Di-siRNA with neuronal (NueN) and glial cells (GFAP) was performed as described previously[50].

RNAseq

Total RNA was isolated from 3 brain punches each from 4 animals per naïve and Di-siRNA^{HTT} treated condition using Monarch® Total RNA Miniprep Kit (NEB, T2010S) following manufacturer protocol. Briefly, tissue was submerged in DNA/RNA protection reagent, homogenized by passing through a 27G hypodermic needle, and incubated for 30 minutes at 55C with proteinase K. RNA was bound to column, subjected to on-column DNase treatment, washed, and eluted in nuclease free water. Library preparation was performed using TruSeq® Stranded mRNA Library Prep (Illumina, 20020594) following manufacturer protocol. Single end sequencing was performed for 75 cycles on the Illumina NextSeq 500, for a total of 271.6 million reads (average of 33.9 million reads per animal).

The resulting 75nt reads were mapped to the cynomolgus macaque genome (Macaca fascicularis 5.0) with STAR/2.5.3a. Reads mapping to annotated exons were counted using HTseq/0.10.0 and differential expression analysis was performed with DESeq2/1.22.2. Genes that had less than 10 reads across all samples or were only expressed in one animal were excluded from further analyses. Seed complementary matches and enriched 6-mers within 3’ UTRs (for genes with annotated 3’ UTRs in Macaca fascicularis Ensembl 95 annotations) were identified using a custom python script. Gene set enrichment analysis was conducted using PANTHER/14.0, conditioning on biological process gene ontology categories.

Statistics

All statistics were calculated using GraphPad Prism 7. Box plots: center line – median, top of box – 75% quartile, bottom of box – 25% quartile, whiskers: minimum and maximum. Additional information can be found in the **Life Sciences Reporting Summary**.

Data availability

The RNA-seq data from non-human primate samples have been deposited in GEO under accession code GSE130132, including processed transcriptome read counts.

Supplementary Material

Refer to Web version on PubMed Central for supplementary material.

ACKNOWLEDGMENTS

This project was funded by NIH/NINDS (R01 NS104022) A.K., NIH/OD (S10 OD020012) A.K., CHDI (Research Agreement A-6119) N.A., Alzheimer's Drug Discovery Foundation (20170101) A.K., Milton-Safenowitz Fellowship (#17-PDF-363) B.M.D.C.G and The Berman-Topper Fund, A.K. and N.A. We would like to thank the University of Massachusetts Medical School Animal Medicine Department and veterinary technicians for their contributions to the large animal studies. We would like to thank Marie-Cecile Didiot for her mouse brain cartoon, Emily Mohn and Samuel Hildebrand for editing the manuscript, and Charles River Laboratories for help with neuropathology.

References

1. Khvorova A & Watts JK The chemical evolution of oligonucleotide therapies of clinical utility. Nat Biotechnol 35, 238–248 (2017). [PubMed: 28244990]
2. Ostergaard ME et al. Efficient Synthesis and Biological Evaluation of 5'-GalNAc Conjugated Antisense Oligonucleotides. Bioconjug Chem 26, 1451–1455 (2015). [PubMed: 26011654]
3. Rajeev KG et al. Hepatocyte-specific delivery of siRNAs conjugated to novel non-nucleosidic trivalent N-acetylgalactosamine elicits robust gene silencing in vivo. Chembiochem : a European journal of chemical biology 16, 903–908 (2015). [PubMed: 25786782]
4. Kordasiewicz HB et al. Sustained therapeutic reversal of Huntington's disease by transient repression of huntingtin synthesis. Neuron 74, 1031–1044 (2012). [PubMed: 22726834]
5. Finkel RS et al. Nusinersen versus Sham Control in Infantile-Onset Spinal Muscular Atrophy. N Engl J Med 377, 1723–1732 (2017). [PubMed: 29091570]
6. Coelho T et al. Safety and efficacy of RNAi therapy for transthyretin amyloidosis. N Engl J Med 369, 819–829 (2013). [PubMed: 23984729]
7. Alterman JF et al. Hydrophobically Modified siRNAs Silence Huntingtin mRNA in Primary Neurons and Mouse Brain. Mol Ther Nucleic Acids 4, e266 (2015). [PubMed: 26623938]
8. Nikan M et al. Docosahexaenoic Acid Conjugation Enhances Distribution and Safety of siRNA upon Local Administration in Mouse Brain. Mol Ther Nucleic Acids 5, e344 (2016). [PubMed: 27504598]
9. Osborn MF & Khvorova A Improving Small Interfering RNA Delivery In Vivo Through Lipid Conjugation. Nucleic Acid Ther (2018).
10. Nikan M et al. Synthesis and Evaluation of Parenchymal Retention and Efficacy of a Metabolically Stable O-Phosphocholine-N-docosahexaenoyl-l-serine siRNA Conjugate in Mouse Brain. Bioconjug Chem 28, 1758–1766 (2017). [PubMed: 28462988]
11. Ly S et al. Visualization of self-delivering hydrophobically modified siRNA cellular internalization. Nucleic Acids Res 45, 15–25 (2017). [PubMed: 27899655]
12. Eckstein F Phosphorothioates, essential components of therapeutic oligonucleotides. Nucleic Acid Ther 24, 374–387 (2014). [PubMed: 25353652]

13. Flierl U et al. Phosphorothioate backbone modifications of nucleotide-based drugs are potent platelet activators. J Exp Med 212, 129–137 (2015). [PubMed: 25646267]
14. Sewing S et al. Assessing single-stranded oligonucleotide drug-induced effects in vitro reveals key risk factors for thrombocytopenia. PloS one 12, e0187574 (2017). [PubMed: 29107969]
15. Crooke ST, Wang S, Vickers TA, Shen W & Liang XH Cellular uptake and trafficking of antisense oligonucleotides. Nat Biotechnol 35, 230–237 (2017). [PubMed: 28244996]
16. Hassler MR et al. Comparison of partially and fully chemically-modified siRNA in conjugate-mediated delivery in vivo. Nucleic Acids Res 46, 2185–2196 (2018). [PubMed: 29432571]
17. Behlke MA Progress towards in vivo use of siRNAs. Mol Ther 13, 644–670 (2006). [PubMed: 16481219]
18. Winkler J, Stessl M, Amartey J & Noe CR Off-target effects related to the phosphorothioate modification of nucleic acids. ChemMedChem 5, 1344–1352 (2010). [PubMed: 20544786]
19. Amarzguioui M, Holen T, Babaie E & Prydz H Tolerance for mutations and chemical modifications in a siRNA. Nucl. Acids Res 31, 589–595 (2003). [PubMed: 12527766]
20. Harborth J et al. Sequence, Chemical, and Structural Variation of Small Interfering RNAs and Short Hairpin RNAs and the Effect on Mammalian Gene Silencing. Antisense & Nucleic Acid Drug Development 13, 83–105 (2003). [PubMed: 12804036]
21. Nair JK et al. Impact of enhanced metabolic stability on pharmacokinetics and pharmacodynamics of GalNAc-siRNA conjugates. Nucleic Acids Res 45, 10969–10977 (2017). [PubMed: 28981809]
22. Fitzgerald K et al. A Highly Durable RNAi Therapeutic Inhibitor of PCSK9. N Engl J Med 376, 41–51 (2017). [PubMed: 27959715]
23. Ray KK et al. Inclisiran in Patients at High Cardiovascular Risk with Elevated LDL Cholesterol. N Engl J Med 376, 1430–1440 (2017). [PubMed: 28306389]
24. Lee YC et al. Binding of synthetic oligosaccharides to the hepatic Gal/GalNAc lectin. Dependence on fine structural features. J Biol Chem 258, 199–202 (1983). [PubMed: 6848494]
25. Roehl I, Schuster M & Seiffert S, Vol. US20110201006 A1 (2011).
26. Liu CC, Liu CC, Kanekiyo T, Xu H & Bu G Apolipoprotein E and Alzheimer disease: risk, mechanisms and therapy. Nat Rev Neurol 9, 106–118 (2013). [PubMed: 23296339]
27. Mahley RW, Weisgraber KH & Huang Y Apolipoprotein E4: a causative factor and therapeutic target in neuropathology, including Alzheimer's disease. Proc Natl Acad Sci U S A 103, 5644–5651 (2006). [PubMed: 16567625]
28. Zetterberg H, Jacobsson J, Rosengren L, Blennow K & Andersen PM Association of APOE with age at onset of sporadic amyotrophic lateral sclerosis. J Neurol Sci 273, 67–69 (2008). [PubMed: 18656208]
29. Didiot MC et al. Nuclear Localization of Huntingtin mRNA Is Specific to Cells of Neuronal Origin. Cell Rep 24, 2553–2560 e2555 (2018). [PubMed: 30184490]
30. Achuta VS et al. Tissue plasminogen activator contributes to alterations of neuronal migration and activity-dependent responses in fragile X mice. The Journal of neuroscience : the official journal of the Society for Neuroscience 34, 1916–1923 (2014). [PubMed: 24478370]
31. Gu X et al. N17 Modifies mutant Huntingtin nuclear pathogenesis and severity of disease in HD BAC transgenic mice. Neuron 85, 726–741 (2015). [PubMed: 25661181]
32. DiFiglia M et al. Huntingtin is a cytoplasmic protein associated with vesicles in human and rat brain neurons. Neuron 14, 1075–1081 (1995). [PubMed: 7748555]
33. Herndon ES et al. Neuroanatomic profile of polyglutamine immunoreactivity in Huntington disease brains. J Neuropathol Exp Neurol 68, 250–261 (2009). [PubMed: 19225411]
34. Weyer A & Schilling K Developmental and cell type-specific expression of the neuronal marker NeuN in the murine cerebellum. Journal of neuroscience research 73, 400–409 (2003). [PubMed: 12868073]
35. Takala RS et al. Glial Fibrillary Acidic Protein and Ubiquitin C-Terminal Hydrolase-L1 as Outcome Predictors in Traumatic Brain Injury. World Neurosurg 87, 8–20 (2016). [PubMed: 26547005]

36. Lind D, Franken S, Kappler J, Jankowski J & Schilling K Characterization of the neuronal marker NeuN as a multiply phosphorylated antigen with discrete subcellular localization. Journal of neuroscience research 79, 295–302 (2005). [PubMed: 15605376]
37. Dou CL, Li S & Lai E Dual role of brain factor-1 in regulating growth and patterning of the cerebral hemispheres. Cereb Cortex 9, 543–550 (1999). [PubMed: 10498272]
38. Janas MM et al. Selection of GalNAc-conjugated siRNAs with limited off-target-driven rat hepatotoxicity. Nature Communications 9, 723 (2018).
39. Birmingham A et al. 3' UTR seed matches, but not overall identity, are associated with RNAi off-targets. Nat Methods 3, 199–204 (2006). [PubMed: 16489337]
40. Zuccato C, Valenza M & Cattaneo E Molecular mechanisms and potential therapeutical targets in Huntington's disease. Physiol Rev 90, 905–981 (2010). [PubMed: 20664076]
41. Evers MM et al. AAV5-miHTT Gene Therapy Demonstrates Broad Distribution and Strong Human Mutant Huntingtin Lowering in a Huntington's Disease Minipig Model. Molecular Therapy 26, 2163–2177 (2018). [PubMed: 30007561]
42. Southwell AL et al. Huntingtin suppression restores cognitive function in a mouse model of Huntington's disease. Sci Transl Med 10 (2018).
43. Pfister EL et al. Artificial miRNAs Reduce Human Mutant Huntingtin Throughout the Striatum in a Transgenic Sheep Model of Huntington's Disease. Hum Gene Ther 29, 663–673 (2018). [PubMed: 29207890]
44. Grondin R et al. Six-month partial suppression of Huntingtin is well tolerated in the adult rhesus striatum. Brain 135, 1197–1209 (2012). [PubMed: 22252996]
45. Tabrizi S et al. Effects of IONIS-HTTRx in Patients with Early Huntington's Disease, Results of the First HTT-Lowering Drug Trial (CT.002). Neurology 90, CT.002 (2018).
46. Bhagat L et al. Novel oligonucleotides containing two 3'-ends complementary to target mRNA show optimal gene-silencing activity. J Med Chem 54, 3027–3036 (2011). [PubMed: 21466154]
47. Malcolm DW, Sorrells JE, Van Twisk D, Thakar J & Benoit DS Evaluating side effects of nanoparticle-mediated siRNA delivery to mesenchymal stem cells using next generation sequencing and enrichment analysis. Bioeng Transl Med 1, 193–206 (2016). [PubMed: 27981244]
48. Wang G, Liu X, Gaertig MA, Li S & Li XJ Ablation of huntingtin in adult neurons is nondeleterious but its depletion in young mice causes acute pancreatitis. Proc Natl Acad Sci U S A 113, 3359–3364 (2016). [PubMed: 26951659]
49. Pfister EL et al. Five siRNAs targeting three SNPs may provide therapy for three-quarters of Huntington's disease patients. Curr Biol 19, 774–778 (2009). [PubMed: 19361997]
50. Godinho B et al. Transvascular Delivery of Hydrophobically Modified siRNAs: Gene Silencing in the Rat Brain upon Disruption of the Blood-Brain Barrier. Mol Ther 26, 2580–2591 (2018). [PubMed: 30143435]

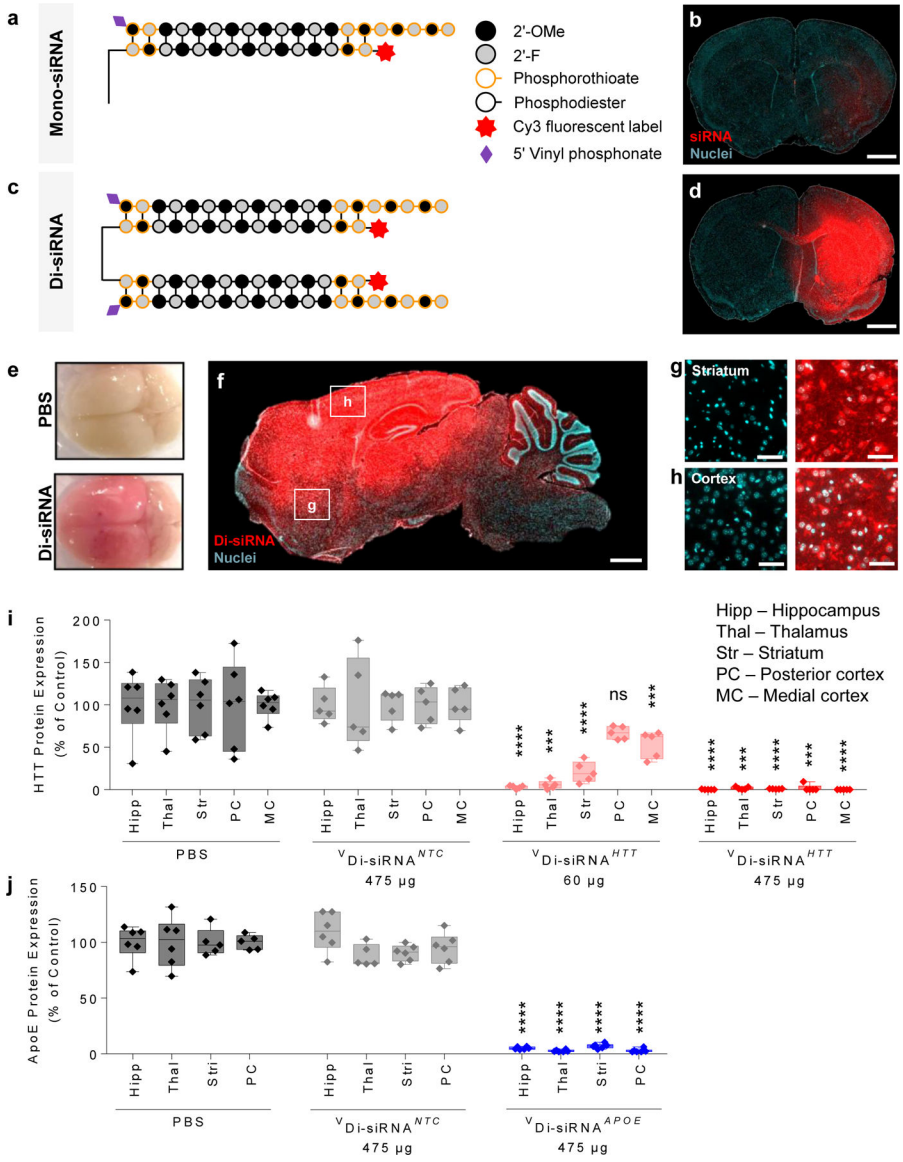

Figure 1. A divalent siRNA chemical configuration enables gene silencing in the mouse brain.

a. Schematic of the chemical structure of Mono-siRNA. **b.** Biodistribution of Cy3-labeled Mono-siRNA 48 hours after a single intrastriatal injection of 50 µg. Scale bar – 1 mm. **c.** Schematic of the chemical structure of Di-siRNA. **d.** Biodistribution of Cy3-labeled Di-siRNA 48 hours after a single intrastriatal injection of 50 µg. Scale bar – 1 mm. **e.** Image of whole mouse brain injected with Di-siRNA (top – PBS, bottom – Di-siRNA) Scale bar – 0.25 cm. **f.** Di-siRNA distributes throughout mouse the brain after a bilateral injection of 475 µg (237 µg/ventricle) into the lateral ventricles. Tiled fluorescent images taken 48 hours post injection. Scale bar – 1 mm. **(g,h)** High resolution images of Di-siRNA distribution to various regions of the mouse brain: **g.** Striatum, **h.** Cortex. Scale bar – 50 µm. **i.** Di-siRNA silences huntingtin (HTT) protein at two different doses in multiple brain regions 1 month after bilateral ICV injection. All statistics are One-Way ANOVA with Dunnett's multiple comparisons test. All results compared to PBS control. Hipp: $F(3,17) = 31.92$, HTT 60µg

****P<0.0001, HTT 457μg ****P<0.0001. Thal: F(3,17) = 16.875, HTT 60μg ***P=0.0003, HTT 457μg ***P=0.0002. Str: F(3,17) = 33.38, HTT 60μg ****P<0.0001, HTT 457μg ****P<0.0001. PC: F(3,17) = 12.64, HTT 457μg ***P=0.0001. MC: F(3,17) = 53.58, HTT 60μg ***P=0.0003, HTT 475 μg ****P<0.0001. PBS: n=6, NTC n=5, HTT 60 μg: n=5, HTT 475 μg: n=5. Mean ± SD. NTC – non-targeting control. **j.** Di-siRNA silences apolipoprotein E (APOE) protein 1 month after bilateral ICV injection. All statistics are One-Way ANOVA with Dunnett's multiple comparisons test. All results compared to PBS control. Hipp: F(2,14) = 1.991, ****P<0.0001. Thal: F(2,14) = 4.283, ****P<0.0001. Str: F(2,15) = 4.781, ****P<0.0001. PC: F(2,14) = 6.618, ****P<0.0001. PBS: n=6. NTC Mean ± SD. NTC – non-targeting control.

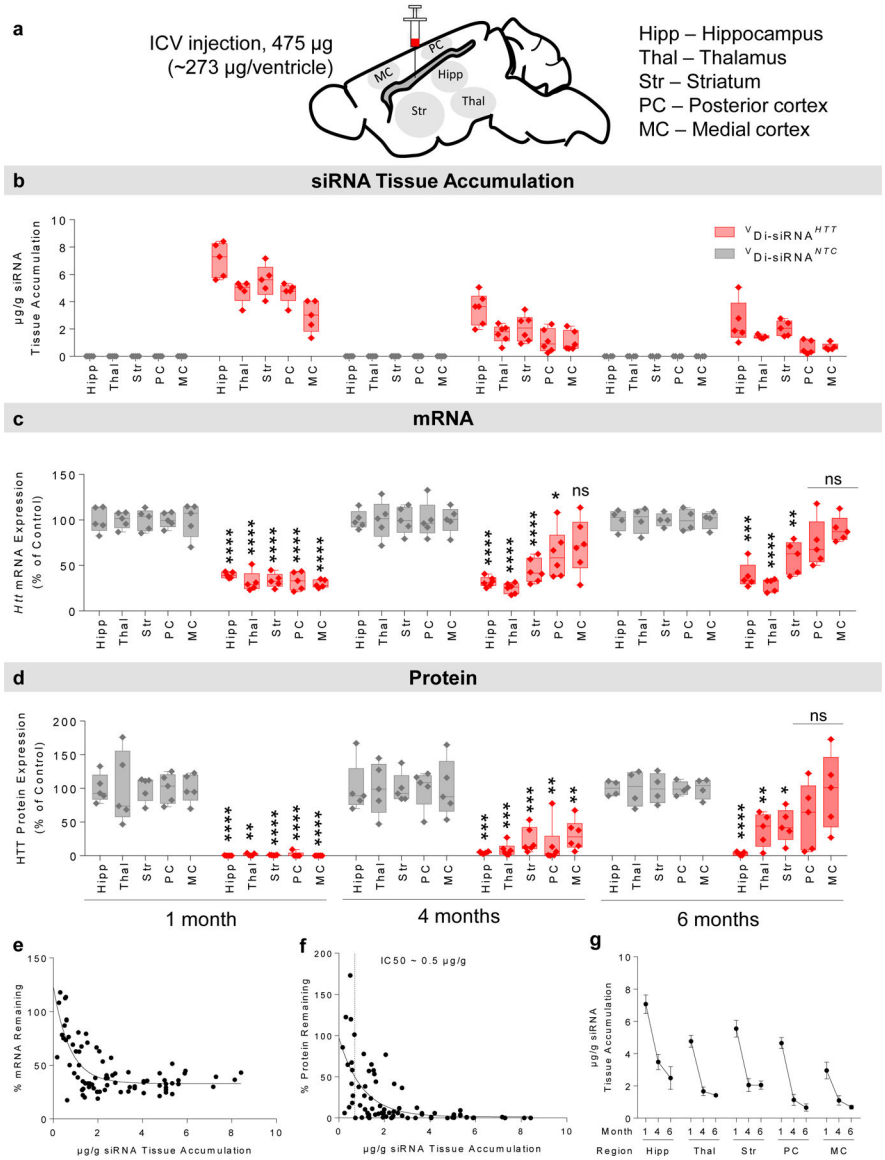

Figure 2. Di-siRNA efficacy is sustained in mice 6 months after a single bilateral ICV injection.

Mice were injected with 475 µg siRNA (bilaterally) (237 µg/ventricle) and data was collected at 1, 4, and 6 months post injection. **a.** Schematic of the duration of effect study in mice. **b.** Guide strand accumulation (µg/g) in five brain regions. **c.** Huntingtin (*Htt*) mRNA silencing (% of control) in five brain regions. All statistics are two-tailed unpaired t-tests. All results compared to NTC control. 1 month. Hipp: t=9.56, df=8, ****p<0.0001. Thal: t=10.59, df=8, ****p<0.0001. Str: t=10.63, df=8, ****p<0.0001. PC: t=11.45, df=8, ****p<0.0001. MC: t=8.082, df=8, ****p<0.0001. HTT: n=5, NTC: n=5. 4 month. Hipp: t=14.26, df=9, ****p<0.0001. Thal: t=8.577, df=9, ****p<0.0001. Str: t=6.606, df=9, ****p<0.0001. PC: t=2.561, df=9, *p=0.0306. HTT: n=6, NTC: n=5. 6 month. Hipp: t=6.998, df=7, ***p=0.0002. Thal: t=9.865, df=7, ****p<0.0001. Str: t=4.264, df=7, **p=0.0037. HTT: n=5, NTC: n=4. **d.** Huntingtin (HTT) protein silencing (% of control) in five brain regions. 1 month. Hipp: t=10.58, df=8, ****p<0.0001. Thal: t=14.092, df=8,

p=0.0035. Str: t=12.05, df=8, ****p<0.0001. PC: t=9.834, df=8, ****p<0.0001. MC: t=10.85, df=8, ****p<0.0001. HTT: n=5, NTC: n=5. 4 month. Hipp: t=6.117, df=9, ***p=0.0002. Thal: t=5.661, df=9, ***p=0.0003. Str: t=6.261, df=9, ***p=0.0001. PC: t=4.651, df=9, **p=0.0012, MC: t=3.46, df=9, **p=0.0072. HTT: n=6, NTC: n=5. 6 month. Hipp: t=19.01, df=7, ****p<0.0001. Thal: t=93.536, df=7, **p=0.0095. Str: t=3.479, df=7, *p=0.0103. HTT: n=5, NTC: n=4. **e. Di-siRNA *Htt* mRNA silencing shows a strong correlation with siRNA guide strand accumulation. **f.** Di-siRNA HTT protein silencing shows a strong correlation with siRNA guide strand accumulation (IC50 ~ 0.5 μg/g). **g.** siRNA guide strand retention shows strong, two phase tissue clearance kinetics. The majority of the compound is cleared within the first month. Clearance slows between 4 and 6 months. Mean ± SD. NTC – non-targeting control.

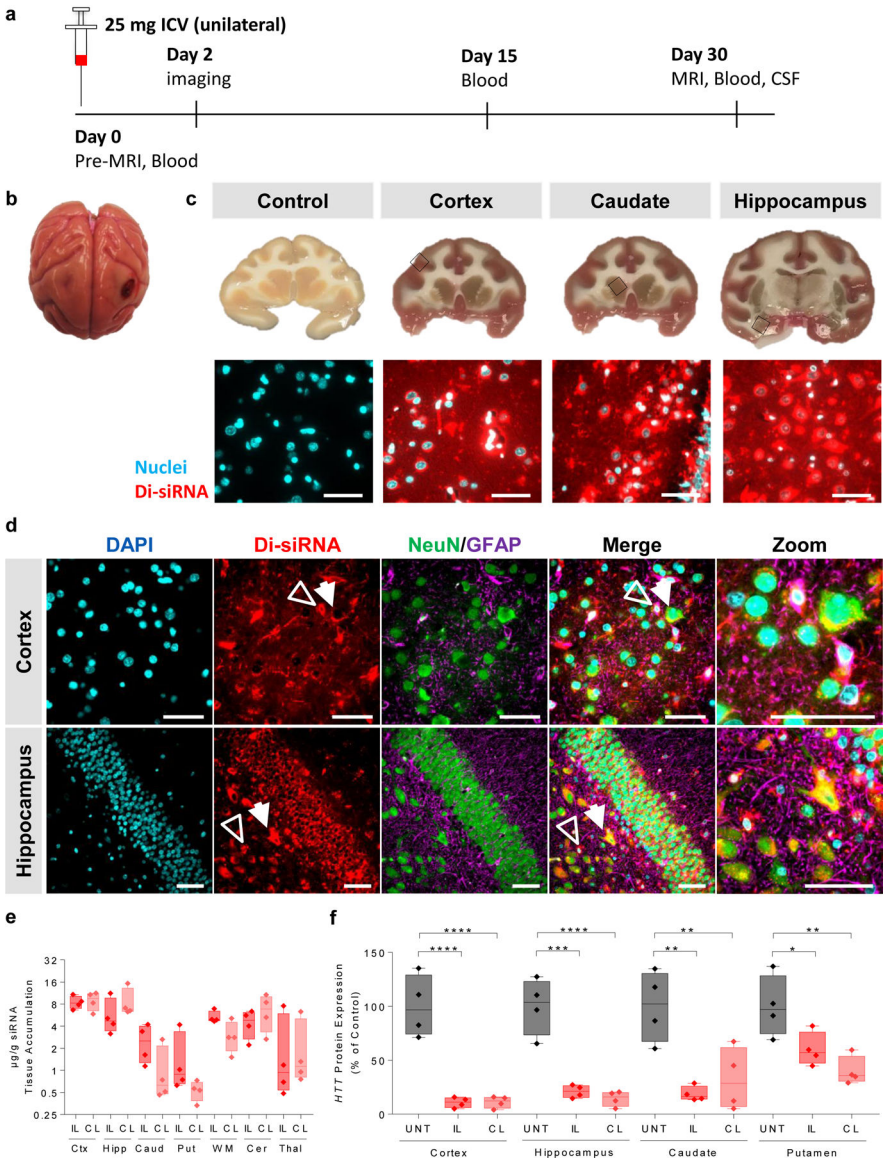

Figure 3. Gene silencing in the non-human primate CNS with Di-siRNAs.

Cynomolgus macaques received a unilateral ICV injection of Di-siRNAs (25 mg). Samples were collected at 48 hours for biodistribution and at 30 days for gene silencing and toxicity assessments. **a.** Schematic of NHP study. **b.** Image of whole NHP brain (left). **c**. Images of NHP brain slices (top). Scale bar – 1 cm. High resolution fluorescent images of Di-siRNA in various regions of the NHP brain (bottom) Scale bar – 50 µm. **d.** Immunofluorescence of the NHP cortex and hippocampus. All images acquired 48 hours after a single unilateral ICV injection of 25 mg Di-siRNA. Hollow arrow indicates glial cells, and closed arrow indicates neurons. Scale bar – 50 µm. **e.** Quantification of siRNA guide strand (n=4 treated animals, µg/g) in seven brain regions, IL – ipsilateral, CL – contralateral. **f.** Huntingtin (HTT) protein silencing (% of control) ipsilateral and contralateral sides of four brain regions. Statistics calculated by One-Way ANOVA with Dunnet's correction for multiple comparisons. All results compared to naïve control. Cortex: $F(2,9) = 35.86$, ****$P<0.0001$. Hippocampus:

F(2,9) = 35.15, ipsilateral ***P = 0.0001, contralateral ****P<0.0001. Caudate: F(2,9) = 11.51, ipsilateral **P = 0.0028, contralateral **P = 0.0087. Putamen: F(2,9) = 9.08, ipsilateral *P = 0.0385, contralateral **P = 0.0043. n=4/group. 1 month (n=4 Di-siRNA treated animals, n=4 naive animals). All graphs are mean ± SD.

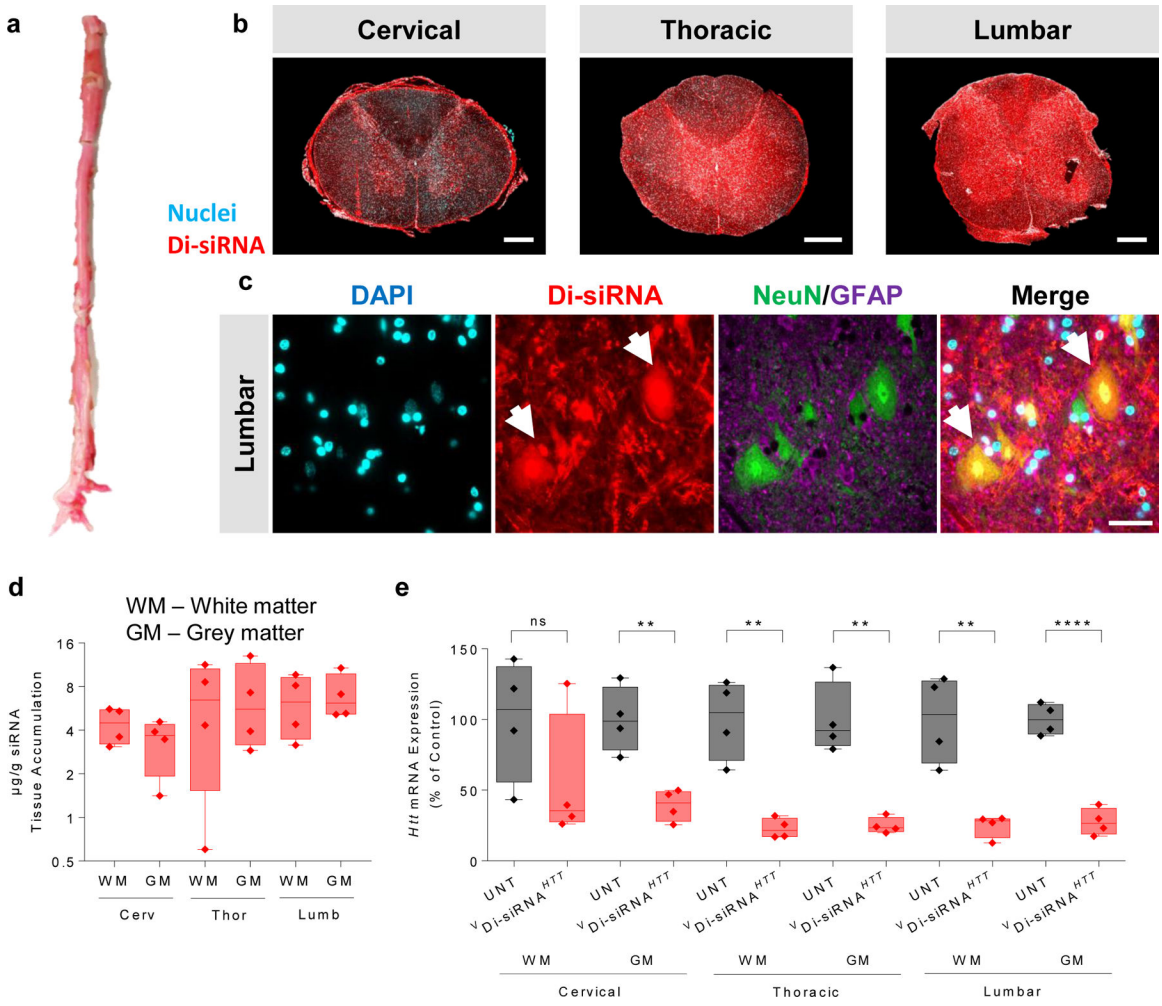

Figure 4. Di-siRNA enables silencing in the spinal cord of non-human primates.

a. Image of the whole NHP spinal cord. **b.** Tiled fluorescent images of cross sections of the spinal cord at each segment. Scale bar – 1 mm. **c**. Immunofluorescence of the NHP spinal cord (cervical, thoracic and lumbar regions). All images acquired 48 hours after a single unilateral ICV injection of 25 mg Di-siRNA. Scale bar – 50 µm. **d.** Quantification of siRNA guide strand (µg/g) in three spinal cord regions, both white and grey matter. **e.** HTT mRNA silencing in various regions of the NHP spinal cord. Statistics calculated by two-tailed unpaired t-test: Cervical GM: t=4.686, df=6, **P=0.0034. Thoracic WM: t= 5.278, df=6, **P=0.0019. Thoracic GM: t=5.757, df=6, **P=0.0012. Lumbar WM: t=4.69, df=6, **P=0.0034. Lumbar GM: t=9.853, df=6, ****P<0.0001. 1 month (n=4 Di-siRNA treated animals, n=4 naive animals). All graphs are mean ± SD.

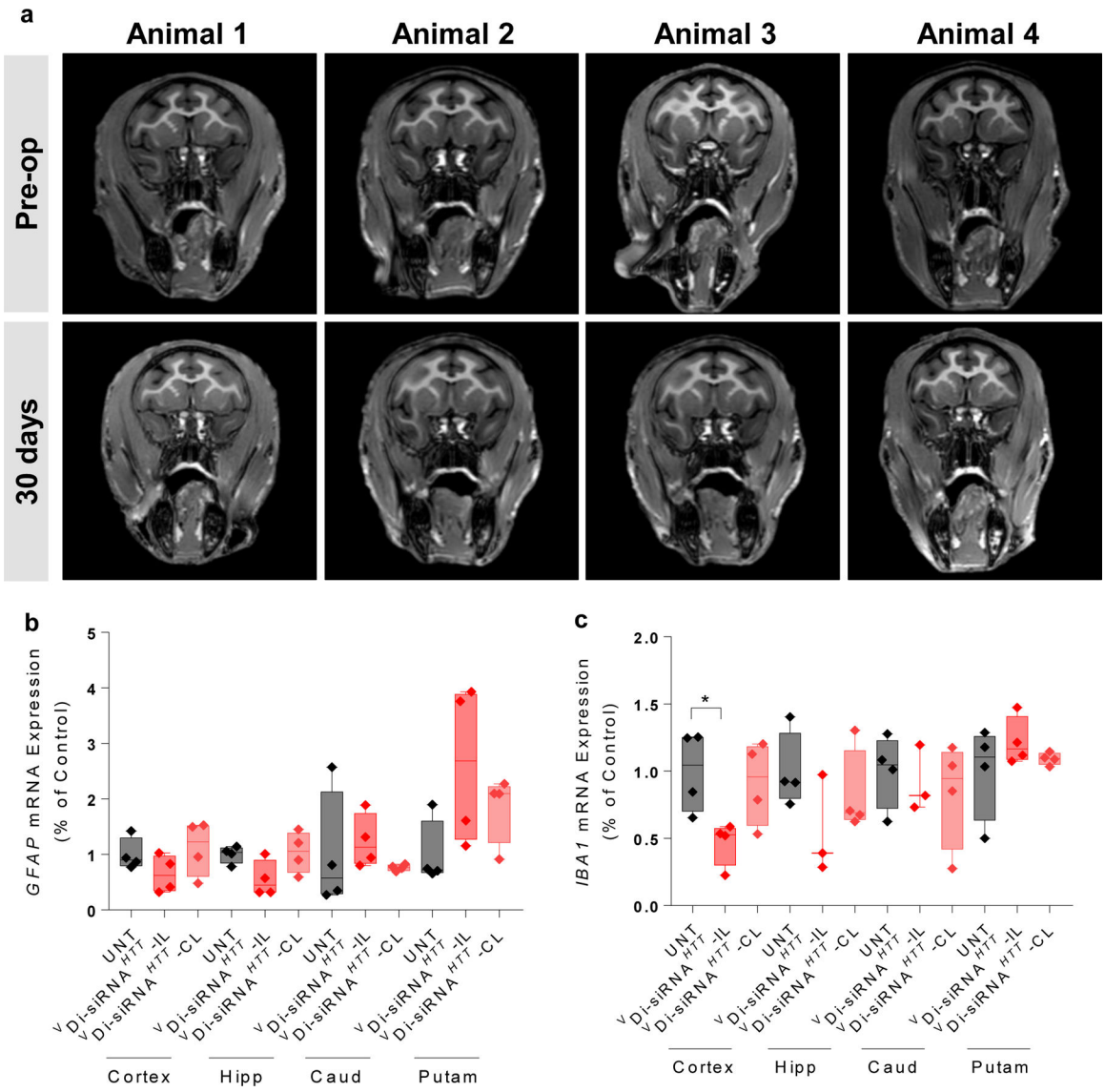

Figure 5. Assessment of brain toxicity 1 month after a single ICV injection of Di-siRNA in non-human primates.

Animals were all dosed with 25 mg Di-siRNA unilaterally into the lateral ventricle. **a.** Pre-operative and post-operative (30 days) MRI scans. **b.** *GFAP mRNA* expression was assessed 30 days after a single ICV injection. **c.** *IBA-1* mRNA expression 30 days after a single ICV injection. Statistics calculated by One-Way ANOVA with Dunnet's correction for multiple comparisons. All results compared to naïve control. F(2,9) = 4.578 iplsilateral *P<0.0359. n=4/group.

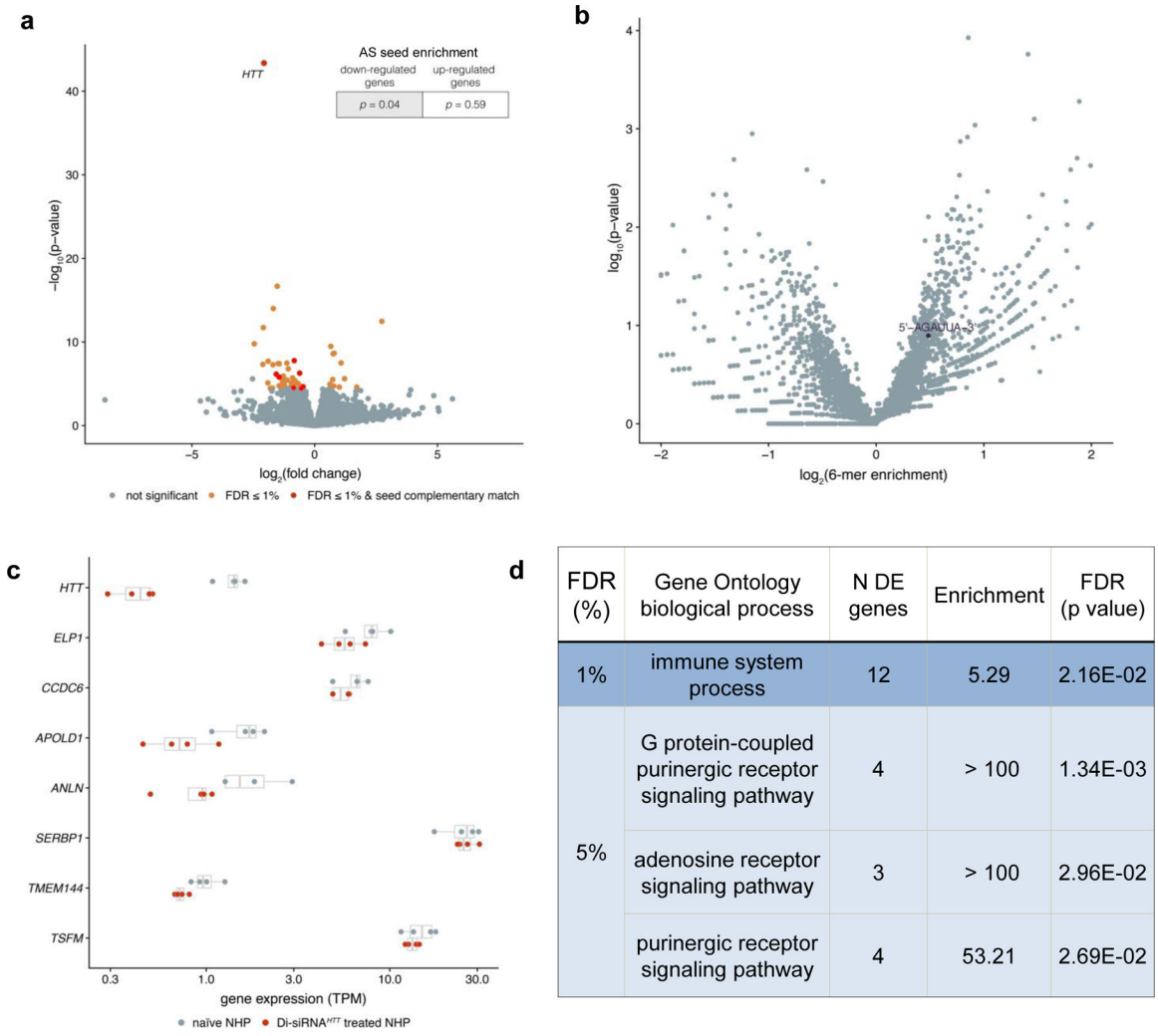

FDR (%)	Gene Ontology biological process	N DE genes	Enrichment	FDR (p value)
1%	immune system process	12	5.29	2.16E-02
5%	G protein-coupled purinergic receptor signaling pathway	4	> 100	1.34E-03
	adenosine receptor signaling pathway	3	> 100	2.96E-02
	purinergic receptor signaling pathway	4	53.21	2.69E-02

Figure 6. RNA-seq shows limited off-target effects of Di-siRNA.

RNA collected from cynomolgus macaques was subjected to RNA-sequencing to assess genome-wide patterns of differential gene expression. **a.** Volcano plot showing genome-wide gene expression changes in Di-siRNA^{HTT}-treated NHPs, with differentially-expressed genes (Benjamini Hochberg FDR < 1%) in orange and differentially-expressed genes with a 3' UTR seed complementary region in red. Enrichment of 3' UTR seed complementarity down- or up-regulated genes (top-right) was calculated using a Fisher's exact test. **b.** Volcano plot showing unbiased screen for enriched 6-mer sequences within 3' UTRs of differentially-expressed gene (FDR < 1%). There are no significantly over- or under-represented sequences after Benjamini Hochberg multiple test correction. Seed complementary sequence for Di-siRNA^{HTT} is indicated in black. **c.** Gene expression measurements (transcripts per million, x-axis) across 4 naïve NHPs (grey) and 4 Di-siRNA^{HTT} treated NHPs (red) for the 8 differentially expressed genes with seed complementary regions. **d.** Significant gene ontology categories for differentially expressed genes with FDR < 1% and FDR < 5%.